

SPIO–RGD nanoparticles as a molecular targeting probe for imaging tumor angiogenesis using synchrotron radiation

Jing Li,^a Chunfu Zhang,^a Ke Yang,^b Ping Liu^{a,*} and Lisa X. Xu^{a,c,*}^aMed-X Research Institute, Shanghai Jiao Tong University, Shanghai, People's Republic of China,^bShanghai Institute of Applied Physics, Chinese Academy of Science, Shanghai, People's Republic of China, and ^cBiomedical Engineering, School of Life Sciences and Biotechnology, Shanghai Jiao Tong University, Shanghai, People's Republic of China. E-mail: pingliu@sjtu.edu.cn,

lisaxu@sjtu.edu.cn

Angiogenesis, new blood vessels sprouting from pre-existing vessels, is essential to tumor growth, invasion and metastasis. It can be used as a biomarker for early stage tumor diagnosis and targeted therapy. To visualize angiogenesis many molecular imaging modalities have been used. In this study a novel X-ray molecular targeting probe using superparamagnetic iron oxide (SPIO) conjugated with arginine–glycine–aspartic acid (SPIO–RGD) has been developed. Based on the extremely high sensitivity to the iron element of synchrotron radiation X-ray fluorescence and the superior spatial resolution of third-generation synchrotron radiation, the feasibility of SPIO–RGD as a promising molecular probe for imaging tumor angiogenesis has been demonstrated.

Received 25 November 2010

Accepted 17 March 2011

© 2011 International Union of Crystallography
Printed in Singapore – all rights reserved**Keywords:** synchrotron radiation X-ray fluorescence imaging; SPIO–RGD; angiogenesis.

1. Introduction

In recent years angiogenesis has become one of the most important and intensely studied areas of cancer research. Angiogenesis, the growth of new capillary blood vessels, is an important component of tumor growth, invasion and metastasis (Folkman, 1971, 1990; Carmeliet & Jain, 2000; Kerbel, 2008). Without a sufficient supply of oxygen and nutrients most tumors cannot grow beyond 2 mm in the absence of angiogenesis (Folkman & Hochberg, 1973). One of the most promising and exciting early stage tumor diagnosis and anti-tumor strategies is based on the visualization and inhibition of angiogenesis *in vivo*. The ability to visualize and quantify angiogenesis will allow early diagnosis and monitoring the angiogenesis states before, during and after adjuvant anti-angiogenic and therapeutic treatments. Thus, angiogenesis can be used as a biomarker and a target for tumor therapy (Matter, 2001; Ferrara & Kerbel, 2005).

Advances in imaging enable us to understand tumor angiogenesis and evaluate the effect of antiangiogenic drugs in animal models and humans. Tumor vascular imaging has been performed clinically by different imaging modalities, such as magnetic resonance imaging (MRI), ultrasound and X-ray computed tomography (CT) imaging. However, visualization of the microvasculature is very challenging even after administration of intravascular contrast agents, because of the limited spatial resolution. The smallest vessels seen *in vivo* are

~100–500 µm (McDonald & Choyke, 2003), and detection for angiogenesis, normally with diameters less than 20 µm, is impossible using these modalities (McDonald & Choyke, 2003; Dobrucki & Sinusas, 2007; Dayton *et al.*, 2004).

With the advent of third-generation synchrotron radiation, synchrotron radiation has become the most promising modality to develop medical imaging. It covers a broad energy band and is much brighter than the conventional X-ray source, allowing for submicrometer spatial resolution (Sun, 2009). Up to now, a lot of work has been performed using synchrotron radiation X-ray angiography. *In vivo* angiography in mouse and rat brains was reported (Kidoguchi *et al.*, 2006; Umetani *et al.*, 2007). Whole-body microvasculature in rats has been investigated with synchrotron radiation microangiography (Liu, Sun *et al.*, 2010). Tumor angiogenesis has also been studied using synchrotron radiation imaging with conventional X-ray contrast agents (Liu, Zhao *et al.*, 2010; Umetani *et al.*, 2009), which may cause severe side effects and are basically not suitable for preclinical research owing to their intrinsic properties (Hainfeld *et al.*, 2006; Christiansen, 2005; Hallouard *et al.*, 2010; Kong *et al.*, 2007; Christiansen *et al.*, 2000).

Imaging of angiogenesis by targeting specific molecular structures is highly desired to increase the sensitivities and specificities of detection. It can also improve the detection limit of small lesions of metastasis and bridge the therapeutic approach of tumors (Costouros *et al.*, 2002; Cai & Chen, 2008; Wong & Kim, 2009). With the submicrometer resolution of

synchrotron radiation X-ray imaging, there are more potential advantages to developing synchrotron radiation X-ray molecular imaging, not only for high sensitivity and high resolution but also for radiation dose reduction, and the capability of real-time three-dimensional dynamic imaging with good soft tissue contrast in deep tissue (Zhou & Brahme, 2010).

Biocompatible nanoparticles have been widely studied in biomedical imaging, providing better contrast and longer circulation times. Surface modification with some target moieties, such as ligands or antibodies, can increase the affinity for target tissue such as tumor angiogenesis (Cormode *et al.*, 2010) and provide functional imaging *in vivo* (Huo *et al.*, 2010; Liu *et al.*, 2009). Recently there have been many kinds of target contrast agents for MRI, positron-emission tomography (PET) and ultrasound molecular imaging (USMI), most based on nanomaterials (Brasch *et al.*, 2000; Schmieder *et al.*, 2005; Winter *et al.*, 2003). Since heavy-element nanoparticles targeting soft tissue can enhance soft tissue contrast, it is now possible to develop new molecular synchrotron radiation imaging in live animals. Thus, synchrotron radiation molecular and functional imaging can be realised when third-generation synchrotron radiation is combined with nanobiotechnology. Recently studies have shown that iron oxide nanoparticles have been detected while accumulated in vessel systems (Rahn, 2009), and gold nanoparticles could be used to target the peripheral lymph node in X-ray imaging (Eck *et al.*, 2010).

In this study superparamagnetic iron oxide nanoparticles with surfaces modified by a short peptide arginine–glycine–aspartic acid (SPIO–RGD) were used in tumor angiogenesis imaging. An H1299 lung cancer subcutaneous tumor model was established in mice. The distribution of iron oxide nanoparticles in H1299 lung cancer was observed using synchrotron radiation X-ray fluorescence (SXRF) imaging at the newly built Shanghai Synchrotron Radiation Facility (SSRF), a third-generation synchrotron radiation facility. The specificity of the targeting was studied.

2. Material and methods

2.1. Nanoparticle probe

Two types of iron oxide nanoparticles were used in this study, superparamagnetic iron oxide (SPIO) and superparamagnetic iron oxide conjugated with a short peptide RGD (SPIO–RGD), which could bind to the integrin $\alpha v \beta 3$ expressed by tumor endothelial cells. The SPIO was prepared through the modified Massart method (Zhang *et al.*, 2007). The average diameter of the nanoparticles was ~ 100 nm. The concentration for the *ex vivo* labeling test was 1 mM, and the concentration for mice-tail vein injection was 36.7 mM.

2.2. H1299 cells co-incubated with a nanoparticle probe

A human lung cancer H1299 cell line was cultured in a six-well plate on glass coverslips for 24 h. After the cells grew on 70% confluence, the culture medium was replaced with a Dulbecco minimum essential medium containing plain SPIO or SPIO–RGD at an iron concentration of 1 mM (310 K, 5%

CO₂). After 4 h of incubation, cells were washed three times with PbS and fixed with methanol for 5 min and acetone for 1 min successively under 353 K. The coverslips were air-dried for 15 min and soaked with PBS for at least 5 min. Slides were incubated with 10% Prussian blue for 5 min, 10% Prussian blue and 20% HCl (1:1) for 30 min, and counterstained with nuclear fast red for 5 min.

2.3. H1299 animal model

Male BALB/c nude mice (20 ± 2 g, 4 weeks) were bought from the Animal Center, CAS, Shanghai, China. They were housed in isolated cages with a 12 h light/dark cycle and fed with sterile food. They were anesthetized using sodium pentobarbital intraperitoneally. All experimental animals were handled following the guidelines provided by the Animal Welfare Committee at the Shanghai Sixth People's Hospital, affiliated to Shanghai Jiao Tong University. An animal bearing subcutaneous H1299 solid tumor was anesthetized by sodium pentobarbital intraperitoneally. The active part of the solid tumor was isolated carefully, excluding any area of necrosis and connective tissues, and cut into small pieces (~ 1 mm³), which were implanted into the flank of the mice under the aseptic procedure (Kozłowski *et al.*, 1984). On the 23rd day after implantation the H1299 solid tumor was about 1.5 cm \times 1.5 cm \times 1.5 cm and used.

2.4. Injection of nanoparticle probe

Mice were divided into three groups: control, SPIO–RGD (targeting) and SPIO (non-targeting) groups. There were three mice in each group. The control group was imaged without nanoparticle treatment. Both the SPIO–RGD and SPIO groups were anesthetized by sodium pentobarbital intraperitoneally. Solutions of SPIO–RGD or SPIO were injected through the tail vein, 200 μ l for each mouse. After 4 h all three groups of the animals were sacrificed and the tumor tissues were harvested followed by the paraffin section procedure.

2.5. SXRF imaging of iron nanoparticles in tumor tissue

All the samples of the three groups were cut into paraffin tissue sections (Leica CM1900 UV), 10 μ m in thickness, mounted on 3525 Ultralene XRF film (SPEX CertiPrep, Metuchen, NJ, USA) and air-dried. For every experimental sample an adjacent section (of the same thickness) was placed on a microscope glass, and was then stained with hematoxylin and eosin (HE) dye. X-ray fluorescence measurements were carried out at the BL15U beamline of the SSRF, China. X-rays of energy 12 keV were focused to a 100 μ m-diameter spot on the specimen. X-ray fluorescence emission was collected by an energy-dispersive Li-ion drifted detector [seven-element Si(Li) detector, e2v]. X-ray fluorescence emission spectra were collected for 6 s.

3. Results

The uptake of SPIO and SPIO–RGD was assessed histologically using Prussian blue staining (Fig. 1). After co-incubation for 4 h a strong uptake of RGD–SPIO was observed (Fig. 1a), whereas there was no significant uptake for SPIO particles in H1299 lung cancer cells (Fig. 1b).

In vivo labeling efficacy was detected through SXRF imaging. Multi-element speciation mapping can be achieved simultaneously, and iron was the element of interest in this study. Figs. 2(a), 2(c) and 2(e) show element maps (Fe) determined by SXRF. Structural information was provided by the adjacent tissue section with HE staining shown in Figs. 2(b), 2(d) and 2(f). The results show that there was no iron distribution in the control tumor tissue (Figs. 2a and 2b). In non-targeting groups (Figs. 2c and 2d) there was a local distribution of iron. SXRF detection (Fig. 2c) agreed with the findings from HE staining (Fig. 2d). The iron was basically in

the region of necrosis (white arrows). As the malignant tumor grew, the central part of the tumor became hypoxic and necrotic. At the margin of necrosis, mature blood vessels were damaged and many red blood cells leaked into the tumor tissue. After being ingested by macrophages, much hemosiderin was left and therefore accumulated in this region. The iron signal could be partly caused by local blood leakage and hemosiderin. Figs. 2(e) and 2(f) show the results of the targeting group. In Fig. 2(e) the distribution of iron is higher on average and is mainly located at the peripheral part of the tumor tissue section. The HE staining result (Fig. 2f) shows that the high concentration of iron shared the same location of vessels (black arrows). The above-mentioned results show that the SPIO–RGD nanoparticles were mostly located in the peripheral blood vessels in tumors where angiogenesis occurred. This indicated the specific binding of SPIO–RGD nanoparticles to the vascular endothelial cells *in vivo*.

4. Summary and discussion

The present study demonstrated that RGD peptide-conjugated superparamagnetic iron oxide (SPIO–RGD) was effective for targeted tumor vascular imaging and could specifically bind to the $\alpha v \beta 3$ integrin on H1299 lung cancer cells. The cell adhesion molecule $\alpha v \beta 3$ integrin is a specific marker of angiogenesis, which is overexpressed in activated and proliferating endothelial cells (Friedlander *et al.*, 1996) and most tumor cells. The integrin $\alpha v \beta 3$ is the most extensively used angiogenesis marker for imaging; RGD specifically binds to $\alpha v \beta 3$ integrin (Brooks *et al.*, 1994). The H1299 cell line is the human lung adenoma cell line, and is epithelial-derived cancerous cells. It has been reported that changes of integrin have been observed in epithelial malignant tumors (Gogali *et al.*, 2004). Our previous studies showed that RGD peptide-conjugated SPIOs could specifically bind to the $\alpha v \beta 3$ integrin on endothelial cells *in vitro* (Gimbrone *et al.*, 1972). In this study only the specific binding ability of RGD to the $\alpha v \beta 3$ integrin on H1299 lung cancer cells was investigated.

SPIO nanoparticles have been used in MRI to achieve a signal decrease in T2-weighted imaging. Our group succeeded in using SPIO–RGD to detect the tumor angiogenesis in MRI imaging (Zhang *et al.*, 2007). Based on our previous study, SPIO–RGD was chosen as a molecular tracer in synchrotron radiation imaging for the purpose of developing molecular tracers for multi-imaging modalities. Through targeting efficacy evaluation in *in vitro* cells and *in vivo* animal models, it was shown that RGD conjugated SPIO nanoparticles can be used as promising molecular targeting probes for angiogenesis in synchrotron radiation X-ray imaging. It is now widely believed that tumor growth is ‘angiogenesis-dependent’. Without angiogenesis, the tumor will remain in dormancy, harmless to the host’s health (Gimbrone *et al.*, 1972). Also, angiogenesis is critical not only to tumor volume expansion but also to malignancy transformation and metastasis. Angiogenesis can be an independent indicator for diagnosis and prognosis.

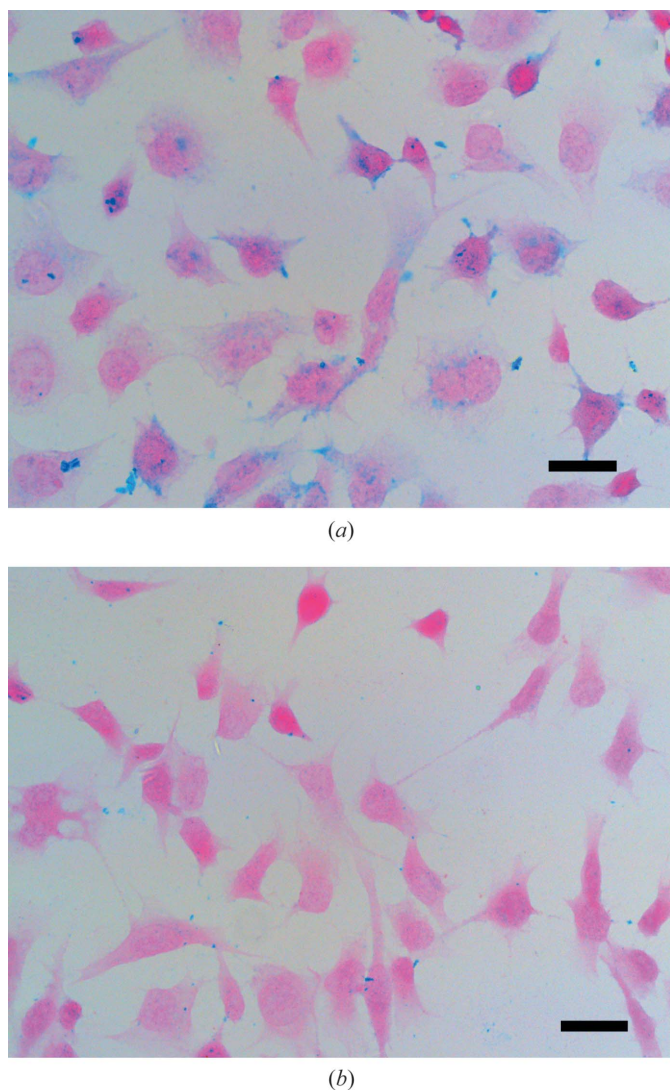


Figure 1
Prussian blue staining of H1299 lung cancer cells co-incubated with (a) SPIO–RGD and (b) SPIO. Blue spots indicate the location of iron. The scale bars in the images represent 50 μm .

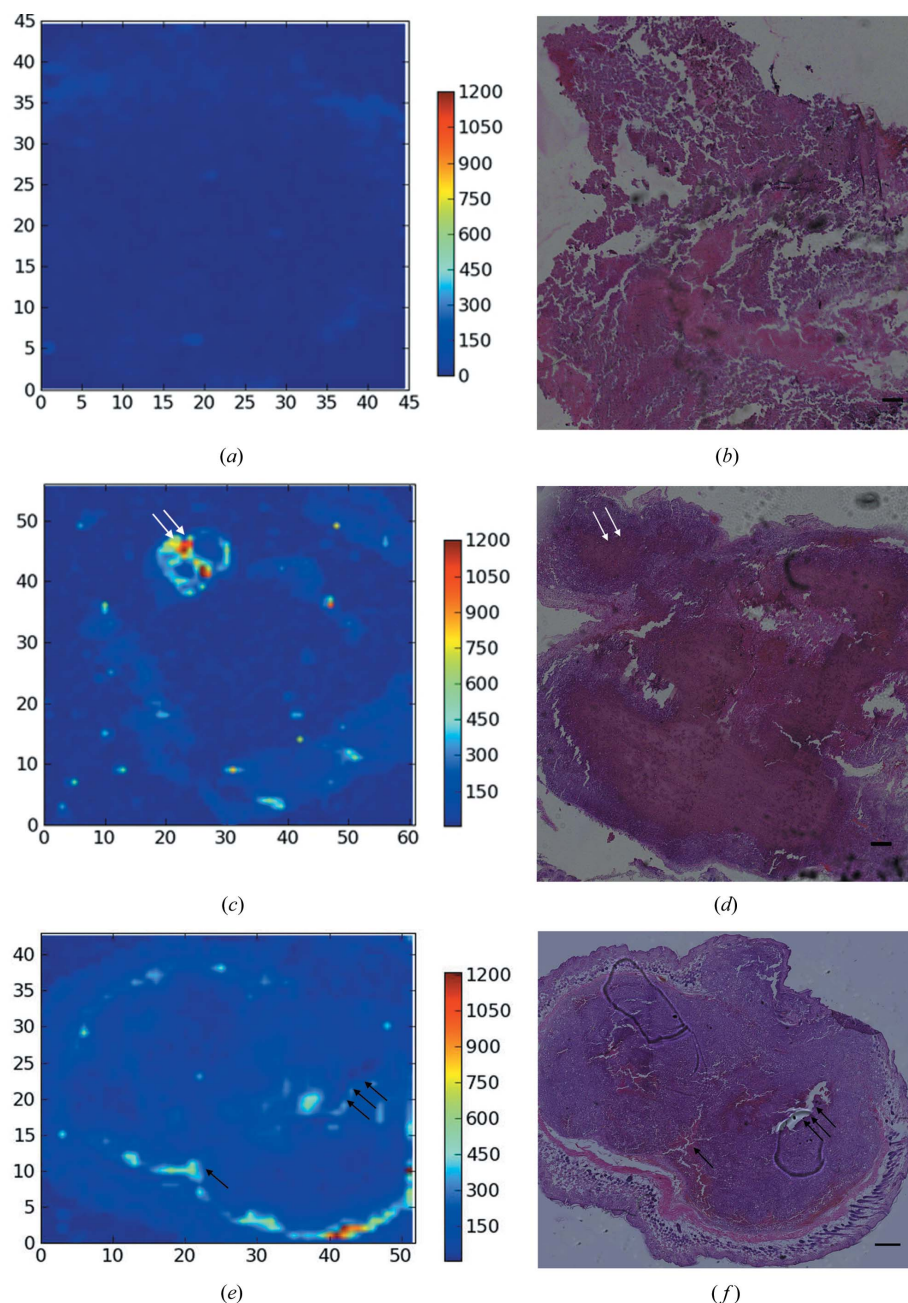


Figure 2
SXRf elemental map (Fe) and the corresponding HE stain of three groups: control [(a) element map, (b) HE stain], non-targeting [(c) element map, (d) HE stain] and targeting [(e) element map, (f) HE stain; the circles are bubbles trapped during the coverslipping procedure]. The transmission images of the HE stain are magnified 100× and the scale bars in the HE stain images represent 200 μm.

Intense efforts have been made in visualizing angiogenesis *in vivo*, involving many modalities, such as PET, SPECT and microbubble-based USMI, MRI. PET has high sensitivity, but its spatial resolution is comparatively poor, requiring image fusion with additional imaging modality, such as CT or MRI. On the other hand, PET tracers are radioactive and have quite a short half-life. USMI has limited resolution and penetration depth; furthermore, the relatively large size of microbubbles also limits the potential application of USMI in tumor angiogenesis imaging. MRI has a much better spatial resolu-

tion than PET, but is sensitive to motion and a lack of molecular probes (Cai & Chen, 2008).

Targeting iron oxide nanoparticles was developed in this study, and the distribution of iron nanoparticles in tumors was observed by synchrotron radiation X-ray fluorescence imaging. The results showed that SPIO-RGD nanoparticles could target tumor blood vessels, and SXRf imaging had a high sensitivity to clusters of nanoparticles in tumor tissue. Although the preliminary results presented in this paper are promising, further investigation is necessary on detection sensitivity and radiation damage to healthy tissue *etc.* to develop a new synchrotron radiation X-ray-based molecular imaging modality *in vivo*.

This work was performed at the BL15U beamline of the Shanghai Synchrotron Radiation Facility (SSRF) in China and was supported by the National Basic Research Program of China (973 Program 2010CB834303), National Natural Science Foundation of China (50725622, 10705020) and the National Basic Research Program of China (2009CB930403).

References

- Brasch, R. C., Li, K. C., Husband, J. E., Keogan, M. T., Neeman, M., Padhani, A. R., Shames, D. & Turetschek, K. (2000). *Acad. Radiol.* **7**, 812–823.
- Brooks, P. C., Clark, R. A. & Cheresch, D. A. (1994). *Science*, **264**, 569–571.
- Cai, W. & Chen, X. (2008). *J. Nucl. Med.* **49**, 113S–128S.
- Carmeliet, P. & Jain, R. K. (2000). *Nature (London)*, **407**, 249–257.
- Christiansen, C. (2005). *Toxicology*, **209**, 185–187.
- Christiansen, C., Pichler, W. J. & Skotland, T. (2000). *Eur. Radiol.* **10**, 1965–1975.
- Cormode, D. P., Jarzyna, P. A., Mulder, W. J. & Fayad, Z. A. (2010). *Adv. Drug Deliv. Rev.* **62**, 329–338.
- Costouros, N., Diehn, F. & Libutti, S. (2002). *J. Cell. Biochem.* **87**, 72–78.
- Dayton, P. A., Pearson, D., Clark, J., Simon, S., Schumann, P. A., Zutshi, R., Matsunaga, T. O. & Ferrara, K. W. (2004). *Mol. Imaging*, **3**, 125–134.
- Dobrucki, L. & Sinusas, A. (2007). *Imaging of Angiogenesis. Cardiac PET and PET/CT Imaging*, pp. 394–411. New York: Springer.
- Eck, W., Nicholson, A., Zentgraf, H., Semmler, W. & Bartling, S. (2010). *Nano Lett.* **10**, 2318–2322.
- Ferrara, N. & Kerbel, R. S. (2005). *Nature (London)*, **438**, 967–974.
- Folkman, J. (1971). *New Engl. J. Med.* **285**, 1182–1186.

- Folkman, J. (1990). *J. Natl. Cancer Inst.* **82**, 4–6.
- Folkman, J. & Hochberg, M. (1973). *J. Exp. Med.* **138**, 745–753.
- Friedlander, M., Theesfeld, C. L., Sugita, M., Fruttiger, M., Thomas, M. A., Chang, S. & Cheresch, D. A. (1996). *Proc. Natl. Acad. Sci. USA*, **93**, 9764–9769.
- Gimbrone, M. A., Leapman, S. B., Cotran, R. S. & Folkman, J. (1972). *J. Exp. Med.* **136**, 261–276.
- Gogali, A., Charalabopoulos, K. & Constantopoulos, S. (2004). *Exp. Oncol.* **26**, 106–110.
- Hainfeld, J. F., Slatkin, D. N., Focella, T. M. & Smilowitz, H. M. (2006). *Br. J. Radiol.* **79**, 248–253.
- Hallouard, F., Anton, N., Choquet, P., Constantinesco, A. & Vandamme, T. (2010). *Biomaterials*, **31**, 6249–6268.
- Huo, T., Du, X., Zhang, S., Liu, X. & Li, X. (2010). *Eur. J. Radiol.* **73**, 420–427.
- Kerbel, R. (2008). *New Engl. J. Med.* **358**, 2039.
- Kidoguchi, K., Tamaki, M., Mizobe, T., Koyama, J., Kondoh, T., Kohmura, E., Sakurai, T., Yokono, K., Kondoh, K. & Umetani, K. (2006). *Stroke*, **37**, 1856–1861.
- Kong, W. H., Lee, W. J., Cui, Z. Y., Bae, K. H., Park, T. G., Kim, J. H., Park, K. & Seo, S. W. (2007). *Biomaterials*, **28**, 5555–5561.
- Kozlowski, J., Fidler, I., Campbell, D., Xu, Z., Kaighn, M. & Hart, I. (1984). *Cancer Res.* **44**, 3522–3529.
- Liu, P., Sun, J., Zhao, J., Liu, X., Gu, X., Li, J., Xiao, T. & Xu, L. X. (2010). *J. Synchrotron Rad.* **17**, 517–521.
- Liu, X., Zhao, J., Sun, J., Gu, X., Xiao, T., Liu, P. & Xu, L. X. (2010). *Phys. Med. Biol.* **55**, 2399–2409.
- Liu, Z., Liu, S., Wang, F., Liu, S. & Chen, X. (2009). *Eur. J. Nucl. Med. Mol. Imaging*, **36**, 1296–1307.
- McDonald, D. M. & Choyke, P. L. (2003). *Nat. Med.* **9**, 713–725.
- Matter, A. (2001). *Drug Discov. Today*, **6**, 1005–1024.
- Rahn, H. (2009). *Nanomedicine*, **4**, 981–990.
- Schmieder, A. H., Winter, P. M., Caruthers, S. D., Harris, T. D., Williams, T. A., Allen, J. S., Lacy, E. K., Zhang, H., Scott, M. J., Hu, G., Robertson, J. D., Wickline, S. A. & Lanza, G. M. (2005). *Magn. Reson. Med.* **53**, 621–627.
- Sun, Z. (2009). *Aust. Med. J.* **1**, 1–5.
- Umetani, K., Kidoguchi, K., Morishita, A., Oizumi, X., Tamaki, M., Yamashita, H., Sakurai, T. & Kondoh, T. (2007). *Conf. Proc. IEEE Eng. Med. Biol. Soc.* pp. 3926–3929.
- Umetani, K., Uesugi, K., Kobatake, M., Yamamoto, A., Yamashita, T. & Imai, S. (2009). *Nucl. Instrum. Methods Phys. Res. A*, **609**, 38–49.
- Winter, P. M., Caruthers, S. D., Kassner, A., Harris, T. D., Chinen, L. K., Allen, J. S., Zhang, H., Robertson, D. J., Wickline, S. A. & Lanza, G. M. (2003). *Cancer Res.* **63**, 5838–5843.
- Wong, F. C. & Kim, E. E. (2009). *Eur. J. Radiol.* **70**, 205–211.
- Zhang, C., Jugold, M., Woenne, E. C., Lammers, T., Morgenstern, B., Mueller, M. M., Zentgraf, H., Bock, M., Eisenhut, W., Semmler, W. & Kiessling, F. (2007). *Cancer Res.* **67**, 1555–1562.
- Zhou, S. A. & Brahma, A. (2010). *Radiat. Prot. Dosim.* **139**, 334–338.